



Biophotonic sensor for rapid detection of brain lesions using 1D photonic crystal

Walaa M. Nouman¹ · S. E.-S. Abd El-Ghany¹ · Samira M. Sallam¹ ·
Abdel-Fattah B. Dawood¹ · Arafa H. Aly² 

Received: 12 February 2020 / Accepted: 13 May 2020
© Springer Science+Business Media, LLC, part of Springer Nature 2020

Abstract

In the present study, we study theoretically the detection of brain lesions by using the defected one-dimensional photonic crystal. The transfer matrix method is used to analyze the optical transmission characteristics of one-dimensional photonic crystals. The device performance is verified by measuring the red shift in resonant wavelength when the refractive index of brain lesions layer changes from 1.3333 to 1.4833. Through the shifting spectrum, the sensitivity of the designed sensor for oligodendrogloma cells reaches to 3080.808 nm/RIU. The high figure of merit [FOM = 6.1×10^7 (1/RIU)] is achieved which evaluates the sensing performance comprehensively.

Keywords Photonic crystals · Optical properties · Brain lesions · Biosensor

1 Introduction

Optical refractive index biosensor is considered one of the fastest developing fields of research. These devices are developed such as surface plasmon resonance (SPR) (Homola et al. 1999; Liedberg et al. 1993), one, two- and three-dimensional photonic crystal (Lee and Fauchet 2007; El Beheiry et al. 2010; Guo et al. 2010), Bragg reflectors (Lin et al. 1997) and long-period fiber grating (Rindorf et al. 2006; Mortensen et al. 2008). Defected photonic crystals PC as sensors depend on resonant wavelength shift which have very sensitivity to the operative refractive index of the cavity defect (Zhao et al. 2015).

There are an estimated 18.1 million new cancer cases (17.0 million excluding nonmelanoma skin cancer) and 9.6 million cancer deaths (9.5 million excluding nonmelanoma skin cancer) (Bray et al. 2018). Thus, it is necessary to improve biosensors to detect such diseases early on.

Depending on refractive indices contrast between cancer and normal cells, photonic crystals are developed to act as a very sensitive and compact size biosensors. 1D-PC sensor which has the structure $[(\text{SiO}_2/\text{air})^n/\text{CDC}/(\text{SiO}_2/\text{air})^n]$ able to detect the cancer

✉ Arafa H. Aly
arafa.hussien@science.bsu.edu.eg; arafa16@yahoo.com

¹ Physics Department, Faculty of Science, Benha University, Benha, Egypt

² TH-PPM Group, Physics Department, Faculty of Science, Beni-Suef University, Beni Suef, Egypt

cells. Where the nanocomposite layers increase the sensitivity to reach to 43 nm/RIU (Ramanujam et al. 2019a). In addition, the photonic crystals may be used as the high sensitivity sensors, refractometric and optoelectronic devices (Shaban et al. 2020; Taya 2018; Ramanujam et al. 2019b). The ternary PC [Si/polymer/SiO₂] are used as temperature sensor (El-Amassi et al. 2018), where the presence of the polymer layer increases the sensitivity.

The used structure is 1D photonic crystal which are composed of air/(SiO₂/PbS)^N/D_d/(SiO₂/PbS)^N/SiO₂. Where N is the number of periodic dielectric materials (SiO₂/PbS) which is considered (N=3). The thickness and refractive indices of these materials are (d₁, d₂, n₁, and n₂) respectively. The defected layer between identical periodic layers was filled with different cancerous cells with thickness D_d=2d_p, 6d_p, 7d_p and 8d_p where d_p is represents the thickness of period. As shown in Fig. 1 the whole structure is surrounded by a SiO₂ substrate from one side and air from another side.

When a defect layer is immersed in the 1D-PC, a transmission resonant peak appears inside the PBG, and its position is a function of the refractive index of the defect layer (Aly et al. 2018). There are various applications on 1D-PC as a sensor whatever in environmental, biological or industrial fields (Sreekanth et al. 2013; Bouzidi et al. 2017; Nair and Vijaya 2010; Abd El-Ghany 2019).

Recently, the sensitivity of 428 nm/RIU for the PC cavity sensor has been experimentally demonstrated by immersing the PC cavity sensor into NaCl solution with different mass concentrations (Zhang et al. 2015). Sensitivity is equal 1100 nm/RIU which is achieved from one-dimensional with a blood sugar layer as a defect layer (Aly et al. 2020). Moreover, a sensitivity of 2200 nm/RIU is obtained by defected 1D-PC of dielectric layers (SiO₂/GaAs) (Aly and Zaky 2019).

In this study, the defected 1D-PC is designed as a biosensor for the brain cancer cells. The normal cells and cancer cells are infiltrated into the PC cavity. As a result, the wavelength shifts of the resonant defect peak in the transmission spectra are computed by the transfer matrix method (TMM).

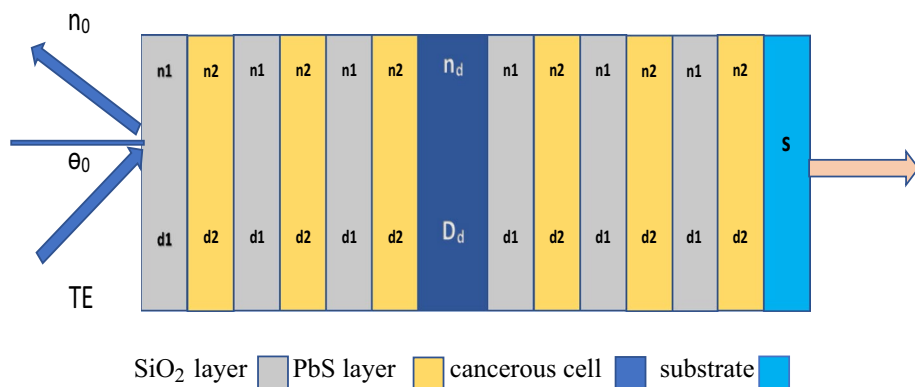


Fig. 1 Schematic simplified representation for 1D defected photonic crystal

2 Theoretical treatment

In Fig. 1, the constituent dielectric materials of designed 1D-PC are the first layer (SiO_2) with thickness $d_1 = 0.06 \mu\text{m}$ and refractive index $n_1 = 1.46$ and the second layer (PbS) with thickness $d_2 = 0.15 \mu\text{m}$ and refractive index $n_2 = 4.2$. The theoretical study of 1D-PC (SiO_2/PbS) was reported previously in the published paper (Sharma et al. 2015). Here the same constituent dielectric materials are used with defected layer is considered brain cancer cells with different refractive indices as shown in the Table 1. When electromagnetic waves incident on the photonic crystal some photons can propagate through the crystal and other photons are expected to be subjected to the total reflection. Thus, the PC acted like the high reflectance reflector for the incident frequencies (Revathy et al. 2019). The forbidden photons with certain frequencies lead to appearance of the photonic band gap (PBG). To realize the PBG through transmission spectra the transfer matrix method was used. In this method, each layer has own matrix with assigning the dielectric parameters and the total transfer matrix of the whole structure is calculated by multiplying the all single layering transfer matrices (Ramanujam et al. 2018). For every layer the transfer matrix method is shown by the following equation:

$$c_K = \begin{pmatrix} \cos \beta_K & \frac{-i}{n_K} \sin \beta_K \\ -in_K \sin \beta_K & \cos \beta_K \end{pmatrix} \quad (1)$$

where K represents the layers of SiO_2 , Pbs or cancerous cells.

The phase angle β_K is listed below:

$$\beta_K = k_K d_K = \frac{2\pi d_K}{\lambda} n_K. \quad (2)$$

where n_K , d_K and k_K are the index of refraction, the thickness of each layer and the wave vector of structure layers.

The single-period matrix which shown in the following equation.

$$C(b) = \begin{pmatrix} C_{11} & C_{12} \\ C_{21} & C_{22} \end{pmatrix} = \begin{pmatrix} \cos \beta_{K1} & \frac{-i}{n_{K1}} \sin \beta_{K1} \\ -jn_{K1} \sin \beta_{K1} & \cos \beta_{K1} \end{pmatrix} \times \begin{pmatrix} \cos \beta_{K2} & \frac{-i}{n_{K2}} \sin \beta_{K2} \\ -jn_{K2} \sin \beta_{K2} & \cos \beta_{K2} \end{pmatrix}. \quad (3)$$

Table 1 Various brain tissues with their refractive indices (Biwas and Gupta 2002)

| Brain tissues | Refractive index |
|---------------------|------------------|
| CSF | 1.3333 |
| Wall of solid brain | 1.3412 |
| Multi sclerosis | 1.3425 |
| Oligodendroglioma | 1.3531 |
| Gray matter | 1.3951 |
| White matter | 1.4121 |
| Low grade glioma | 1.4320 |
| Medulloblastoma | 1.4412 |
| Glioblastoma | 1.4470 |
| Lymphoma | 1.4591 |
| Metastasis | 1.4833 |

Since $b=(d_1+d_2)$ is the lattice constant. And,

$$c_{11} = \cos \beta_{K1} \cos \beta_{K2} - \frac{r_1}{r_2} \sin \beta_{K1} \sin \beta_{K2}. \quad (4a)$$

$$c_{12} = \frac{-i}{r_1} \sin \beta_{K1} \cos \beta_{K2} - \frac{i}{r_2} \cos \beta_{K1} \sin \beta_{K2}. \quad (4b)$$

$$c_{21} = -ir_1 \sin \beta_{K1} \cos \beta_{K2} - ir_2 \cos \beta_{K1} \sin \beta_{K2} \quad (4c)$$

$$c_{22} = \cos \beta_{K1} \cos \beta_{K2} - \frac{r_1}{r_2} \sin \beta_{K1} \sin \beta_{K2}. \quad (4d)$$

and;

$$r_1 = n_{K1} \cos \theta_{K1}, \quad r_2 = n_{K2} \cos \theta_{K2}$$

For TE wave, whereas

$$r_1 = \frac{\cos \theta_{K1}}{n_{K1}}, \quad r_2 = \frac{\cos \theta_{K2}}{n_{K2}}$$

For TM wave.

For the whole structure of N periods and by using Chebyshev polynomials (Mason and Handscomb 2003), the total characteristic transfer matrix M can be obtained by:

$$M(Nb) = (M_A M_B)^N (M_D) (M_A M_B)^N = \begin{pmatrix} M_{11} & M_{12} \\ M_{21} & M_{22} \end{pmatrix}. \quad (5)$$

where A , B and D are the SiO_2 layer, Pbs layer and defected layer of cancerous cells, respectively. And N is the no. of periodic layers.

Finally, the transmittance of the whole structure is given by:

$$T = \frac{p_f}{p_0} |t^2|. \quad (6)$$

where,

$$p_0 = \sqrt{\frac{\epsilon_0}{\mu_0}} n_{fo} \cos \theta_o. \quad (7)$$

$$p_f = \sqrt{\frac{\epsilon_0}{\mu_0}} n_f \cos \theta_f. \quad (8)$$

and t is the transmission coefficient which h is given by

$$t = \frac{2p_0}{((M_{11} + p_f M_{12} p_0) + M_{21} + p_f M_{22})}. \quad (9)$$

3 Results and discussions

One of the most significant biophysical parameters is the index of refraction for cells. Refractive indices of normal and abnormal cells were measured and correlated to values of diseases such as cancer, malaria, anemia, bacterial infection, etc. (Liu et al. 2016). Brain tumors are expected to be deadly and crucially effect on the quality of patient life. In the United States, almost 700,000 people who live with a primary brain tumor. In 2019, nearly 86,970 people are diagnosed as primary brain (www.braintumor.org). When brain lesions have refractive indices less than 1.395 such as multiple sclerosis (1.3425) or solid brain abscess near the wall (1.341) are considered as benign. Otherwise, brain lesions which have a refractive index (RI) greater than 1.412 were expected to be malignant. This means that, the malignancy degree is directly proportional to the RI of lesions (Biswas and Luu 2009).

RI of a solution with 100% distilled water is 1.333 which is considered as an external reference and is compared to CSF as an internal reference. According to Gladstone–Dale law (Effron 2002) the refractive index of brain lesions is directly proportional to physical density (gm/cm^3) of protein/lipid contents and versus to water content in the tissues (Biwas and Gupta 2002; Biswas et al. 2017).

We have used the wavelength range from 1.5 to 4.5 μm which is matched to infrared. When the defected layer is filled with CSF tissues, the photonic band gap is formed from 1.766 to 3.76 μm and with the width is 1.994 μm but in the case of metastasis tissues, the PBG is red shifted with the width is 1.872 μm and formed in the range from 1.887 to 3.759 μm . The large width of PBG appears due to the high contrast in refractive indices between SiO_2 and Pbs layers. Also, the resonant peak through the PBG is red shifted as the refractive index of cancerous cells increases. The resonant peak is shifted to eliminate changes in the effective refractive index of the structure to keep the optical path difference be constant and the resonant condition of the standing wave is unchanged. The changes in the thickness of the defected layer affect the resonant peak shift and thus affect the sensor sensitivity. In the current calculations, the defected layer thickness is allowed with the following values 0.42, 1.26, 1.47 and 1.68 μm at normal incident light as shown in Table 2.

Table 2 Peak wavelength (μm) for different brain cell cancerous at various values of defected layer thickness (μm)

| Index of refraction (n) | Peak position at $D_d=0.42$ (μm) | Peak position at $D_d=1.26$ (μm) | Peak position at $D_d=1.47$ (μm) | Peak position at $D_d=1.68$ (μm) |
|-------------------------|---|---|---|---|
| 1.3333 | 2.397 | 2.302 | 2.64 | 2.977 |
| 1.3412 | 2.407 | 2.314 | 2.654 | 2.992 |
| 1.3425 | 2.408 | 2.316 | 2.656 | 2.995 |
| 1.3531 | 2.421 | 2.332 | 2.674 | 3.015 |
| 1.3951 | 2.472 | 2.395 | 2.746 | 3.096 |
| 1.4121 | 2.492 | 2.42 | 2.776 | 3.129 |
| 1.4320 | 2.516 | 2.45 | 2.81 | 3.167 |
| 1.4412 | 2.526 | 2.463 | 2.825 | 3.185 |
| 1.4470 | 2.533 | 2.472 | 2.835 | 3.196 |
| 1.4591 | 2.548 | 2.49 | 2.856 | 3.219 |
| 1.4833 | 2.576 | 2.526 | 2.897 | 3.265 |

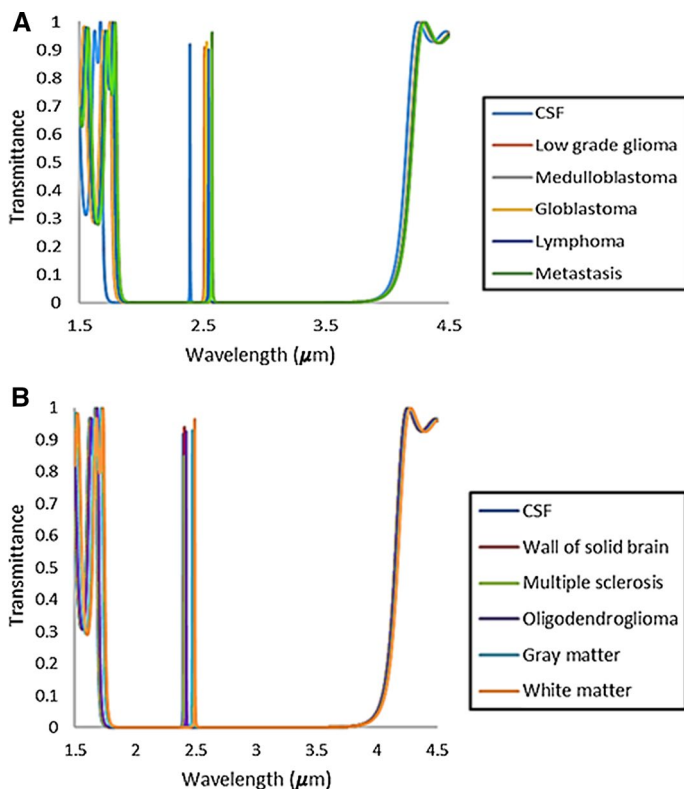


Fig. 2 Transmittance when the defected layer filled with different types of brain cancerous cells at $D_d = 0.42 \mu\text{m}$

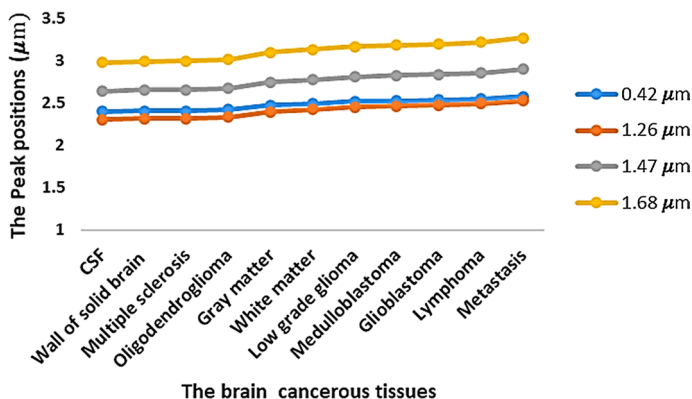


Fig. 3 Illustrates the shift in the peak position which is caused by the different defected layer thickness D_d

At $D_d = 0.42 \mu\text{m}$, the resulted transmission spectrum from the PC sensor for different types of brain lesions is shown in Fig. 2a, b. The wavelength of resonant peak is shifted to the longest wavelength with increasing D_d as shown in Fig. 3. At the higher value of D_d than

1.68 μm , we found that the shift in the resonant peak is decreased. As shown in Table 2, at $D_d = 1.68 \mu\text{m}$, there is the longest shift in the wavelength. The resonant peak for CSF appears at 2.977 μm in Fig. 4a, b with shifting to 3.265 μm for metastasis as shown in Fig. 4b.

A significant factor demonstrates the efficiency of sensor is called the sensitivity. The sensitivity of refractive index sensor is considered that the value of wavelength shift divided by the changed RI of defected layer as in the following equation (Biswas and Luu 2009; Mariotto 2011) (Table 3).

$$S = \frac{\Delta\lambda}{\Delta n} \quad (10)$$

where $\Delta\lambda$ is the wavelength shift of peak resonance caused by the changing of Δn . By considering the wavelength of resonant peak and RI of normal cell as a reference, we found that $\Delta\lambda = (\lambda_{\text{cancerouscell}} - \lambda_{\text{normalcell}}) \Delta n = (n_{\text{cancerouscell}} - n_{\text{normalcell}})$. Table 4 shows the effect of the defected layer thickness on the sensitivity average of the sensor. The high sensitivity appears when the thickness of defected layer is 1.68 μm at a normal incident as shown in Fig. 5. For the same defected layer thickness, the sensitivity for different brain lesions is increases once and decreases again. Since the sensitivity is a ratio between two variables at once the numerator ($\Delta\lambda$) increases and again the denominator (Δn) increases.

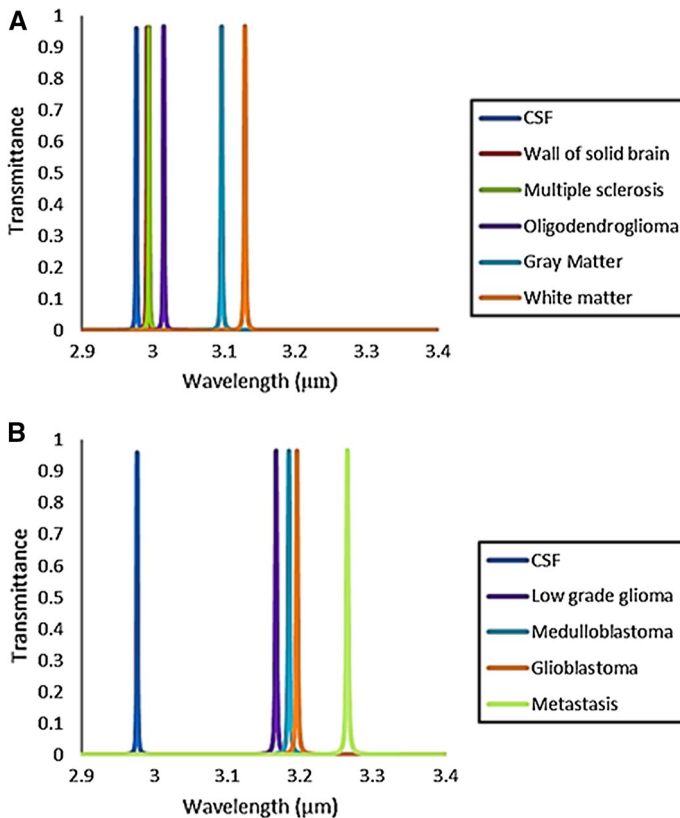


Fig. 4 The resonant peaks for brain lesions when the thickness of defected layer is $D_d = 1.68 \mu\text{m}$ at $\theta = 0^\circ$

Table 3 The sensitivity (nm/RIU) of different brain cells cancerous at different values of defected layer thickness (μm) and $\theta=0^\circ$

| Index of refraction (n) | Sensitivity at $D_d=0.42$ (μm) | Sensitivity at $D_d=1.26$ (μm) | Sensitivity at $D_d=1.47$ (μm) | Sensitivity at $D_d=1.68$ (μm) |
|-------------------------|---|---|---|---|
| 1.3333 | | | | |
| 1.3412 | 1265.823 | 1518.987 | 1772.152 | 1898.734 |
| 1.3425 | 1195.652 | 1521.739 | 1739.13 | 1956.522 |
| 1.3531 | 1212.121 | 1515.152 | 1717.172 | 1919.192 |
| 1.3951 | 1213.592 | 1504.854 | 1715.21 | 1925.566 |
| 1.4121 | 1205.584 | 1497.462 | 1725.888 | 1928.934 |
| 1.4320 | 1205.674 | 1499.493 | 1722.391 | 1925.025 |
| 1.4412 | 1195.551 | 1492.122 | 1714.551 | 1927.711 |
| 1.4470 | 1196.13 | 1495.163 | 1715.04 | 1926.121 |
| 1.4591 | 1200.318 | 1494.436 | 1717.011 | 1923.688 |
| 1.4833 | 1193.333 | 1493.333 | 1713.333 | 1920 |

Table 4 The average of sensitivity (nm/RIU) at different thickness of defected layer (D_d)

| Thickness of defected layer, D_d (μm) | The sensitivity average, S (nm/RIU) |
|--|-------------------------------------|
| 0.42 | 1208.378 |
| 1.26 | 1503.274 |
| 1.47 | 1725.188 |
| 1.68 | 1925.147 |

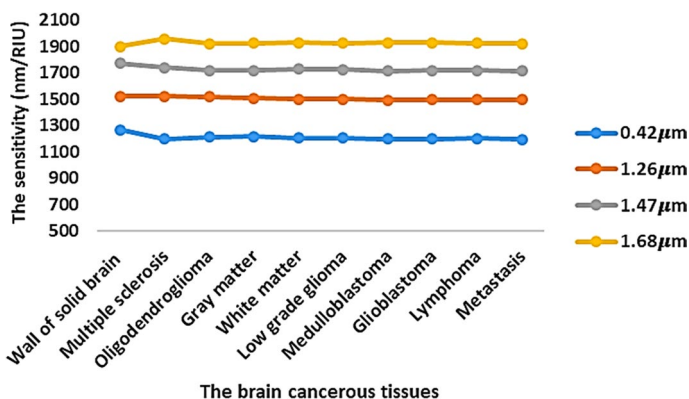


Fig. 5 Illustrates the effect of the different values of defected layer thickness on the sensitivity

The impact of the different light incident angles on the resonant defect peak is noted to obtain a high sensitivity sensor. In the current work, the incident angles have the following values 10° , 20° , 30° , 40° , 50° , 60° , 70° and 80° while keeping the defected layer thickness remains fixed as $1.68 \mu\text{m}$. As shown in Fig. 6, the high sensitivity is

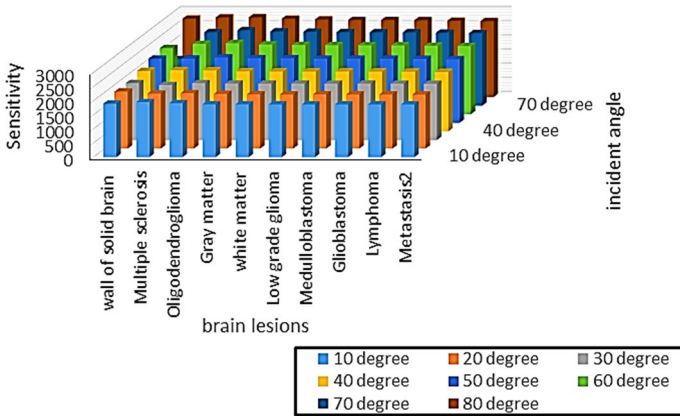


Fig. 6 The sensitivity of 1D-PC with the defected layer thickness $D_d=1.68 \mu\text{m}$ when incident angle $\theta=10^\circ, 20^\circ, 30^\circ, 40^\circ, 50^\circ, 60^\circ, 70^\circ$ and 80°

obtained when $\theta=80^\circ$. So, the designed PC sensor is $[\text{Air}/(\text{SiO}_2/\text{PbS})^3/D_d/(\text{SiO}_2/\text{PbS})^3/\text{SiO}_2]$ with the defected layer thickness is $1.68 \mu\text{m}$ at incident angle 80° .

Table 5 shows the important parameters of RI sensor which are used in the detection of the sample characteristics. The detection limit (DL) able to characterize the smallest change in RI for a sample. DL is calculated by division the sensor resolution (R) by the sensor sensitivity (S) (Biswas and Luu 2009).

$$DL = \frac{R}{S} \tag{11}$$

where R is the smallest spectral shift, which can be measured:

Table 5 Sensitivity parameter S, FOM, SNR, R and DL for designed 1D-PC sensor for various cancerous cells

| RI of brain lesions | $\Delta\lambda_{\text{res}}$ (nm) | $\Delta\lambda_{1/2}$ (nm) | S (nm/RIU) | FOM (1/RIU) | SNR | R (nm) | DL (RIU) |
|---------------------|-----------------------------------|----------------------------|-----------------|-------------------|----------|-------------|-------------|
| 1.3333 | | | | | | | |
| 1.3412 | 0.024 | 8E-05 | 3037.975 | 37,974,684 | 300 | 1.2815E-05 | 4.21827E-09 |
| 1.3425 | 0.028 | 9E-05 | 3043.478 | 33,816,425 | 311.1111 | 1.42864E-05 | 4.6941E-09 |
| 1.3531 | 0.061 | 5E-05 | 3080.808 | 61,616,162 | 1220 | 5.64013E-06 | 1.83073E-09 |
| 1.3951 | 0.185 | 1E-05 | 2993.528 | 27,213,886 | 1681.818 | 1.14513E-05 | 3.82537E-09 |
| 1.4121 | 0.235 | 3E-05 | 2982.234 | 22,940,258 | 1807.692 | 1.32914E-05 | 4.45686E-09 |
| 1.4320 | 0.291 | 5E-05 | 2948.328 | 19,655,522 | 1940 | 1.50678E-05 | 5.11062E-09 |
| 1.4412 | 0.317 | 5E-5 | 2937.905 | 19,586,036 | 2113.333 | 1.47488E-05 | 5.02019E-09 |
| 1.4470 | 0.334 | 6E-05 | 2937.555 | 18,359,719 | 2087.5 | 1.57805E-05 | 5.372E-09 |
| 1.4591 | 0.367 | 7E-05 | 2917.329 | 17,160,759 | 2158.824 | 1.66266E-05 | 5.69925E-09 |
| 1.4833 | 0.434 | 2E-04 | 2893.333 | 14,466,667 | 2170 | 1.95355E-05 | 6.75189E-09 |

$$R = \frac{\Delta\lambda_{1/2}}{1.5 * (SNR)^{1/4}}. \quad (12)$$

$\Delta\lambda_{1/2}$ is the spectral half width of the transmission dip. SNR is the signal to noise ratio which is shown by (Effron 2002).

$$SNR = \frac{\Delta\lambda_{res}}{\Delta\lambda_{1/2}}. \quad (13)$$

where, $\Delta\lambda_{res}$ is the wavelength shift of resonant peak. The figure of merits (FOM) is the ability of sensor to detect any variations in the peak of the resonance which is defined as:

$$FOM = \frac{S}{\Delta\lambda_{1/2}}. \quad (14)$$

The transmission spectrum of the proposed designed device shows that the wavelength of resonant peak is increase with increasing RI of cancerous cell. This relation is represented by Fig. 7 and the following equation:

$$\lambda_d = 2904.4 \times (n_d)^2 - 1807 \quad (15)$$

$$R^2 = 0.9998. \quad (16)$$

where λ_d is the resonant wavelength (nm) which related to index of refraction n_d . R^2 value is between the fitting and the theoretical calculations. When R^2 is equal to 1, this mean that the sensitivity of biosensor is very high.

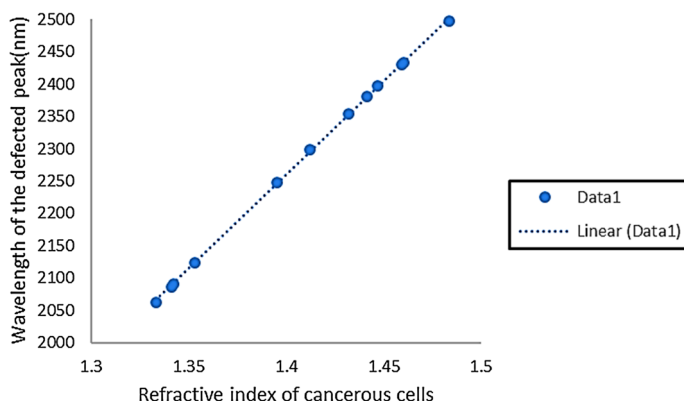


Fig. 7 The relation between refractive index of cancerous cells and the wavelength of resonant peaks

4 The detection of multiple sclerosis and Glioblastoma in brain lesions

By the magnetic resonance (MR) scanner, the relaxation map T_2 is prepared for a normal persons and patients with different grades of multiple sclerosis and glioblastoma (Mason and Handscomb 2003). The value of T_2 for brain lesions tissues is directly proportion to its water content and given by the following equation:

$$Y = 0.0765 \times T_2 + 68.481. \quad (17)$$

where Y denotes a fraction of accumulated water. T_2 is a spin-spin relaxation time that through its transverse magnetization decay (Biwas and Gupta 2002; Biswas et al. 2017). From refractive index mapping of brain (Ramanujam et al. 2018; Mason and Handscomb 2003; Liu et al. 2016), the index of refraction for tissues is related to the proportion of solid component and its content of water. There is inverse relationship between RI value and T_2 value of tissue as shown in the following equation:

$$n = \left(\frac{4.338}{T_2} \right) + 1.3338. \quad (18)$$

where n is the RI for tissues. In the brain lesions such as glioblastoma and metastasis, T_2 values still low due to the little water content and increased the solid components. And therefore, RI of these lesions is high because of increased removal lipids that appears from the tissue necrosis and membrane collapse (Ito et al. 2002). Diagnosis or discrimination can be determined from RI values that have higher accuracy more than other parameters (White and Fan 2008). By using different values of RI for the same brain lesions as Glioblastoma and Multiple sclerosis lesions in the defected layer of biosensor. We can obtain the red shift in the resonant peaks with an increase in RI, as shown in Figs. 8 and 9.

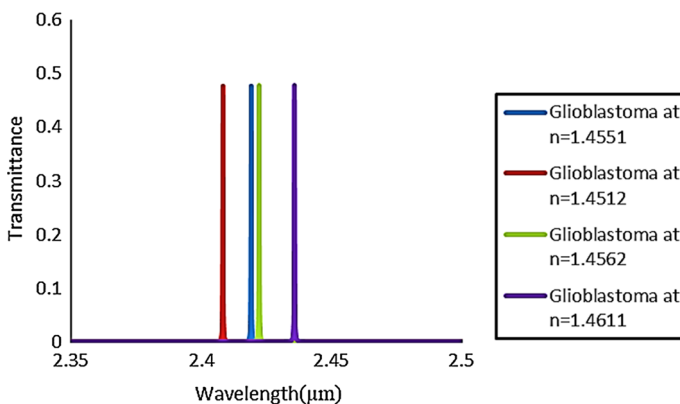


Fig. 8 The resonant peaks for 1D-PC with the defected layer $D_d = 1.68 \mu\text{m}$ at incident angle $\theta = 80^\circ$ for different glioblastoma cells

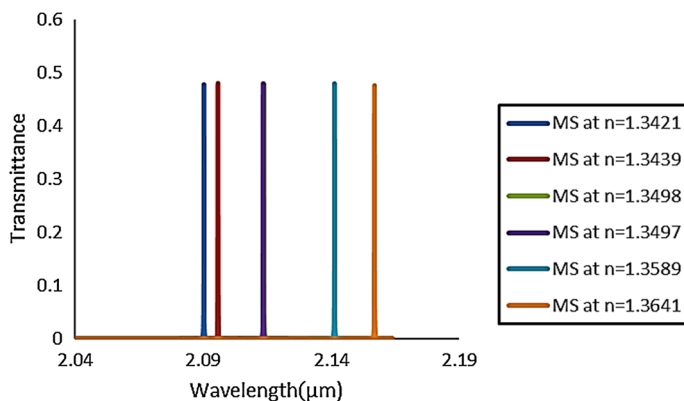


Fig. 9 The resonant peaks for 1D-PC with the defected layer $D_d = 1.68 \mu\text{m}$ at incident angle $\theta = 80^\circ$ for multiple sclerosis (MS) cells

5 Conclusion

Here we have theoretically designed defected 1D-PC as RI sensor for the brain lesions. We studied the transmission spectrum of 1D-PC sensor based on the transfer matrix method. At $D_d = 1.68 \mu\text{m}$ and $\theta = 80^\circ$, the structure of PC sensor $[\text{Air}/(\text{SiO}_2/\text{PbS})^3/\text{D}/(\text{SiO}_2/\text{PbS})^3/\text{SiO}_2]$ appears a high sensitivity. The resulted transmission spectrum for the designed sensor shows that the resonant defect peak is red shifted from 2.063 to 2.497 as the brain lesions replace from CSF with $n = 1.3333$ to metastasis with $n = 1.4833$. The sensitivity of designed sensor is ranged from low value (2893.333) nm/RIU for metastasis cell to a high value (3080.808) nm/RIU for oligodendroglioma. Therefore, DL of this sensor is very low which in order 10^{-9} (RIU). The high value of FOM is reaches to $6.16 * 10^7$ (1/RIU) which means that the high sensing ability to detect a change in the resonant peak. Glioblastoma and Multiple sclerosis tissues with different densities could be detected by our PC sensor. Through the transmission spectrum, the resonant peak is red shifted when the RI changed from (1.4512 to 1.4611) and (1.3421 to 1.3641) for glioblastoma and multiple sclerosis tissues, respectively.

References

- Abd El-Ghany, S.E.-S.: Analysis of temperature sensors based on ternary one dimensional photonic crystals with double defects. *J. Nanoelectron. Optoelectron.* **14**, 1532–1538 (2019)
- Aly, A.H., Zaky, Z.A.: Ultra-sensitive photonic crystal cancer cells sensor with a high-quality factor. *Cryogenics* **104**, 102991 (2019)
- Aly, A.H., Ameen, A.A., ElSayed, H.A., Mohamed, S.H.: Photonic crystal defective superconductor and black body radiations. *Opt. Quant. Electron.* **50**, 1–12 (2018)
- Aly, A.H., Zaky, Z.A., Shalaby, A.S., Ahmed, A.M., Vigneswaran, D.: Theoretical study of hybrid multi-functional one-dimensional photonic crystal as a flexible blood sugar sensor. *Phys. Scr.* **95**(3), 035510 (2020)
- Biswas, T., Luu, T.: In vivo MR measurement of refractive index, relative water content and T2 relaxation time of various brain lesions with clinical application to discriminate brain lesions. *Int. J. Radiol.* **13**, 1–9 (2009)

- Biswas, T.K., Bandopadhyay, R., Dutta, A.: Validating the discriminating efficacy of MR T2 relaxation value of different brain lesions and comparison with other differentiating factors: use of artificial neural network and principal component analysis. *Int. J. Radiol.* **20**, 1–20 (2017)
- Biwas, T.K., Gupta, A.K.: Retrieval of true color of the internal organ of CT images and attempt to tissue characterization by refractive index: initial experience. *Indian J. Radiol. Imaging* **12**, 169–178 (2002)
- Bouzidi, A., Bria, D., Falyouni, F., Akjouj, A., Lévêque, G., Azizi, M., Berkhli, H.: A biosensor based on one-dimensional photonic crystal for monitoring blood glycemia. *J. Mater. Environ. Sci.* **8**, 3892–3896 (2017)
- Bray, F., Ferlay, J., Soerjomataram, I., Siegel, R.L., Torre, L.A., Jemal, A.: Global cancer statistics 2018: GLOBOCAN estimates of incidence and mortality worldwide for 36 cancers in 185 countries. *CA Cancer J. Clin.* **68**, 394–424 (2018)
- Effron, N.: *Contact Lenses A-Z*, vol. 159. Butterworth-Heinemann, Oxford (2002)
- El Beheiry, M., Liu, V., Fan, S., Levi, O.: Sensitivity enhancement in photonic crystal slab biosensors. *Opt. Express* **18**, 22702–22714 (2010)
- El-Amassi, D.M., Taya, S.A., Vigneswaran, D.: Temperature sensor utilizing a ternary photonic crystal with a polymer layer sandwiched between Si and SiO₂ layers. *J. Theor. Appl. Phys.* **12**, 293–298 (2018)
- Guo, Y., Ye, J.Y., Divin, C., Huang, B., Thomas, T.P., Baker Jr., J.R., Norris, T.B.: Real-time biomolecular binding detection using a sensitive photonic crystal biosensor. *Anal. Chem.* **82**(12), 5211–5218 (2010)
- Homola, J., Yee, S.S., Gauglitz, G.: Surface plasmon resonance sensors: review. *Sens. Actuators B Chem.* **54**, 3–15 (1999)
- Ito, K., Saito, K., Taniguchi, T., Yoshimura, H.: Temperature distribution in and around array applicator for interstitial microwave hyperthermia combined with interstitial radiation therapy. In: *Proceedings of 27th International URSI General Assembly*, Maastricht (2002)
- Lee, M., Fauchet, P.M.: Two-dimensional silicon photonic crystal based biosensing platform for protein detection. *Opt. Express* **15**, 4530–4535 (2007)
- Liedberg, B., Lundstrom, I., Stenberg, E.: Principles of biosensing with an extended coupling matrix and surface plasmon resonance. *Sens. Actuators B Chem.* **11**, 63–72 (1993)
- Lin, V.S.Y., Motesarei, K., Dancil, K.P.S., Sailor, M.J., Ghadiri, M.R.: A porous silicon-based optical interferometric biosensor. *Science* **278**, 840–843 (1997)
- Liu, P.Y., Chin, L.K., Ser, W., Chen, H.F., Hsieh, C.M., Lee, C.H., et al.: Cell refractive index for cell biology and disease diagnosis: past, present and future. *Lab Chip* **16**(4), 634–644 (2016)
- Mariotto, A.B., Yabroff, K.R., Shao, Y., Feuer E.J., Brown, M.L.: Projections of the cost of cancer care in the United States: 2010–2020. *J. Natl. Cancer Inst.* **103**(2), 117–128 (2011)
- Mason, J.C., Handscomb, D.C.: *Chebyshev Polynomials*. Chapman & Hall/CRC, Boca Raton (2003)
- Mortensen, N.A., Xiao, S., Pedersen, J.: Liquid-infiltrated photonic crystals—enhanced light-matter interactions for lab-on-a-chip applications. *Microfluid. Nanofluid.* **4**, 117–127 (2008)
- Nair, R.V., Vijaya, R.: Photonic crystal sensor: an overview. *Prog. Quantum Electron.* **34**, 89–134 (2010)
- Ramanujam, N.R., Amiri, I.S., Taya, S.A., Olyae, S., Udaiyakumar, R., Pandian, A.P., Wilson, K.J., Mahalakshmi, P., Yupapin, P.P.: Enhanced sensitivity of cancer cell using one dimensional nano composite material coated photonic crystal. *Microsyst. Technol.* **25**, 1–19 (2018)
- Ramanujam, N.R., Amiri, I.S., Taya, S.A., Olyae, S., Udaiyakumar, R., Pandian, A.P., et al.: Enhanced sensitivity of cancer cell using one dimensional nano composite material coated photonic crystal. *Microsyst. Technol.* **25**, 189–196 (2019a)
- Ramanujam, N.R., El-Khozondarb, H.J., Dhasarathan, V., Taya, S.A., Aly, A.H.: Design of one dimensional defect based photonic crystal by composited superconducting material for bio sensing applications. *Phys. B* **572**, 42–55 (2019b)
- Revathy, V., Boopathi, C.S., Selvakumar, K., Wilson, K.S.J., Taya, S.A., Aly, A.H., Rajan, M.M.: Nonlinear polarization in metal nanocomposite system based photonic crystals. *Optik* **176**, 78–84 (2019)
- Rindorf, L., Jensen, J.B., Dufva, M., Pedersen, L.H., Høiby, P.E., Bang, O.: Photonic crystal fiber long-period gratings for biochemical sensing. *Opt. Express* **14**, 8224–8231 (2006)
- Shaban, S.M., Mehane, A., Aly, A.H.: Determination of 1-propanol, ethanol, and methanol concentrations in water based on a one-dimensional photonic crystal sensor. *Appl. Opt.* **59**(13), 3878–3885 (2020)
- Sharma, S., Kumar, R., Singh, K.S., Kumar, A., Kumar, V.: Omnidirectional reflector using linearly graded refractive index profile of 1D binary and ternary photonic crystal. *Optik* **126**, 1146–1149 (2015)
- Sreekanth, K.V., Zeng, S., Yong, K.-T., Yu, T.: Sensitivity enhanced biosensor using graphene-based one-dimensional photonic crystal. *Sens. Actuators, B* **182**, 424–428 (2013)
- Taya, S.A.: Ternary photonic crystal with left-handed material layer for refractometric application. *Opto Electron. Rev.* **25**, 236–241 (2018)
- White, I.M., Fan, X.: On the performance quantification of resonant refractive index sensors. *Opt. Express* **16**, 1020–1028 (2008)

- Zhang, Y., Han, S., Zhang, S., Liu, P., Shi, Y.: High-Q and high-sensitivity photonic crystal cavity sensor. *IEEE Photonics J.* **7**, 1–6 (2015)
- Zhao, Y., Zhang, Y.-N., Lv, R.-Q.: Simultaneous measurement of magnetic field and temperature based on magnetic fluid-infiltrated photonic crystal cavity. *IEEE Trans. Instrum. Meas.* **64**, 1055–1062 (2015)

Publisher's Note Springer Nature remains neutral with regard to jurisdictional claims in published maps and institutional affiliations.